# *Projection lithography patterned high-resolution quantum dots/thiol-ene photo-polymer pixels for color down conversion*



**As Published:** 10.1364/OE.27.030864

**Publisher:** The Optical Society

**Persistent URL:** https://hdl.handle.net/1721.1/136500

**Version:** Final published version: final published article, as it appeared in a journal, conference proceedings, or other formally published context

Research Article | Vol. 27, No. 21 / 14 October 2019 / Optics Express 30864
Optics EXPRESS

# Projection lithography patterned high-resolution quantum dots/thiol-ene photo-polymer pixels for color down conversion

XINHAO LI,[1] DARSHAN KUNDALIYA,[2] ZHENG JIE TAN,[1] MARIA ANC,[2] AND NICHOLAS X. FANG[1,*]

[1]Department of Mechanical Engineering, Massachusetts Institute of Technology, 77 Massachusetts Ave, Cambridge, MA 02139, USA
[2]OSRAM Opto Semiconductors Inc., 71 Cherry Hill Drive, Beverly, MA 01915, USA
[*]nicfang@mit.edu

**Abstract:** Pixelated color converters are envisioned to achieve full-color high-resolution display through down conversion of blue/ultraviolet(UV) micro-LEDs. Quantum dots (QDs) are promising narrow-band converters of high quantum efficiency and brightness enabling saturated colors with wide color gamut in displays. Here we demonstrate high-resolution pixelated red and green QDs/thiol-ene photo-polymer converters (single pixel down to 6 μm; converters array of 21 μm pixel, 30 μm pitch and sub 10 μm thickness) patterned through projection lithography. QDs capped with amine surface group are uniformly dispersed in thiol-ene photo-polymer matrix at high concentrations (up to 100 mg/mL), which reduces aggregation and improves conversion efficiency by 0.5-1 times compared to drop-cast QDs. Color cross-talk is also reduced through patterning light blocking walls between converter pixels.



## 1. Introduction

Down conversion of blue/UV micro-LEDs with sub-100 μm pixel size to emit longer-wavelength colors draws increasingly attention, for the broad applications including high-resolution wide-gamut display, [1–3] automotive adaptive front-lighting, [4,5] high bandwidth visible light communication [6–8] and spectral/spatial-sensitive optogenetic stimulation. [9–11] Quantum dots (QDs) outperform other down conversion materials due to their high efficiency, tunable narrow-band emission, broad absorption spectra and fast photoluminescence (PL) decay times. [12–14] Patterning QDs color converters on blue/UV micro-LEDs can also simplify the manufacturing procedure and reduce product defect rate compared to integrating red, green and blue emitting micro-LEDs on a single chip. [15–17] Ink jet, [18,19] aerosol jet [16,20] and photo-lithography [17,21,22] methods have been applied to pattern QDs converters on blue/UV micro-LEDs with sub-100 μm pixel size. However, challenges still remain to generate high resolution color-selective patterns compatible with the advanced III-Nitride blue/UV micro-LEDs with pitch and pixel size approaching ~10 μm, [3,23,24] meanwhile to mitigate the drop of photoluminescnese (PL) due to aggregation at high QDs loads and host material effects. [25]

Ink jet and aerosol jet printing rely on solvent based drop casting with nozzles followed by solvent removal. These methods have only been able to pattern QDs pixels with limited size of ~50 μm. [16,20] Meanwhile, the aggregation of QDs and coffee-ring effects after solvent evaporation lowers the light conversion efficiency and emission uniformity. [20,25] Due to the fluidity of the solution-phase QDs ink, the patterned pixels are usually limited to circular shapes, [18,19] and color cross-talk may happen during the patterning process. [16] Furthermore, ink jet and aerosol jet printing are not efficient, for the low patterning speed (up to 200 μm/s) of these serial methods. [18]

#373752 https://doi.org/10.1364/OE.27.030864
Journal © 2019 Received 25 Jul 2019; revised 15 Sep 2019; accepted 19 Sep 2019; published 10 Oct 2019

Optics EXPRESS

Conventional photo-lithography patterning requires multiple steps of thermal treatments and developer washing to pattern QDs/photoresists composites with high-resolution of ~20 μm pixel size. [17,21,22] High QD loading in thin films is required to achieve full conversion of blue/UV light. [26,27] However, the aggregation of highly concentrated QDs during polymerization of the polar photoresists can increase scattering and non-radiative decay mechanisms, which reduces the PL efficiency. [17,26] Besides, the incompatibility between QDs and photoresists, also known as host material effects, can cause the degradation of QDs' surface passivation, [28] which further reduce the PL efficiency and lowers the re-usability of QDs suspended in uncured photoresists. Furthermore, the omnidirectional emission of QDs raises the issue of color cross-talk due to unintentional excitation from light leakage and coupling through the sides of nearby pixels. [29]

The aforementioned issues call the careful choice for patterning techniques along with host materials for QDs color converters. In this paper, we demonstrated direct projection lithography of pixelated red and green QDs/thiol-ene photo-polymer composite with a UV digital light processing (DLP) printer for color down conversion of blue LEDs. The DLP projection lithography provides a scalable and air-processing patterning procedure with high-resolution. We were able to achieve sub 25 μm square pixels array with 30 μm pitch and sub 10 μm thickness. The smallest pixel size can go down to 6 μm with the DLP printing setup. Meanwhile a wide view angle approaching the Lambertian emission profile and 95% color gamut coverage of DCI-P3 standard are achievable. The choice of thiol-ene photo-polymer as the host material and quantum dots capped with amine surface groups facilitates the uniform dispersion of QDs in the cured polymer matrix, reduces aggregation and partially mitigates the drop of PL efficiency. Compared with drop-casting method, the QDs/NOA86 composite improves PL quantum yield (PLQY) by 0.5-1 times at high QDs loads (25 to 100 mg/mL). Furthermore, we also demonstrated color cross-talk reduction by through projection lithography pattering of light absorbing walls between nearby pixels.

## 2. Materials and methods

### 2.1. Synthesis of QDs/photo-polymer composite

NOA86 from Norland Optics was used as the photo-polymer matrix in this study. Green (QSP-520) and red (QSP-620) emission CdSe/Zns core-shell QDs powder capped with octadecylamine surface group were purchased from Ocean Nanotech. QDs powder was firstly dispersed in chloroform (≥ 99%, Sigma Aldrich) to 5 mg/mL. Then NOA86 were added to form QDs/NOA86 composite with final concentration of 25, 50, 75 and 100 mg/mL after chloroform removal under reduced pressure.

### 2.2. Direct patterning with projection lithography

The components schematic of the projection lithography printing system are shown in Fig. 1(a). It contains an inverted optical microscope (IX71, Olympus) with 2-axis motorized stage system (ProScan III, Prior Scientific) of sub 0.1 μm positioning resolution, a DLP projector (PRO4500, Wintech) with 405 nm UV LED and high-resolution digital micro-mirror device (DMD) as the light source and dynamic mask. Patterns reflected by the DMD was guided by the optics and focused through the 20X/0.25 objective lens (Olympus) onto the 2-axis printing stage. The optics was aligned so that the optical path between the DMD and the objective lens is the same as the optical path between the observing CCD and the objective lens. Therefore the system could fulfill pattern alignment and UV projection simultaneously.

Figure 1(b) shows the schematic of patterning procedures of red and green QDs color converters on blue micro-LEDs array. QDs/NOA86 composite (5 μL in experiment) is drop-cast onto the substrate, followed by chloroform removal under reduced ambient pressure. The QDs/NOA86 composite forms a thin layer of liquid film over the printing area, as in subplots II and IV. UV exposure of the pixel pattern cures the thin layer of the QDs/NOA86 composite under the projected

Optics EXPRESS

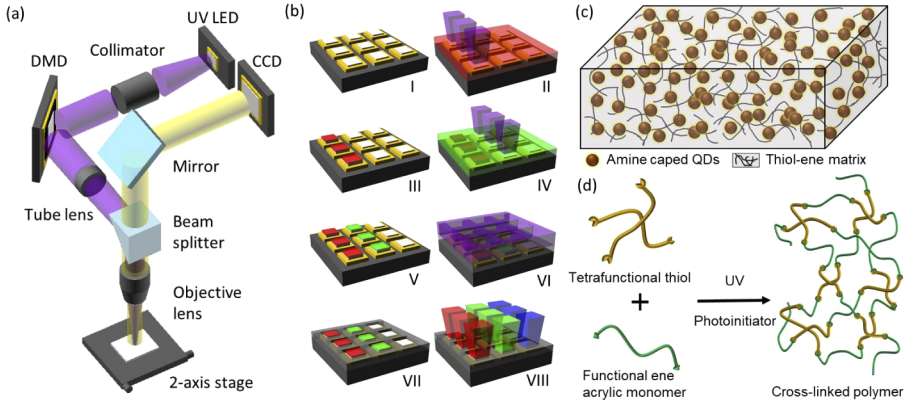


**Fig. 1.** (a) Schematic of the UV DLP projection lithography printing system. (b) Schematic of patterning procedure of red (I-III) and green (IV-V) color converters on blue micro-LED array with black matrix (VI-VII) for RGB full color display (VIII). UV pattern projections are shown as the purple square beams. (c) Schematic microstructure of QDs/NOA86 composite films, consisting of cross-linked thiol-ene polymer matrix and amine capped QDs. (d) Schematic of thiol-ene reaction under UV initiation to form the polymer matrix.

area. The uncured composite is rinsed away with IPA and the substrate is blow dried with air, resulting in the pixelated color converters, as shown in subplots III and V. Figure 1(c) shows the microstructure of cured NOA86 thin films with high QDs load. The thiol-ene reaction process is shown in Fig. 1(d). NOA86 contains tetrafunctional thiol, acrylic monomers with at least 2 -ene functional groups and UV/visible sensitive photoinitiator (proprietary formula/ingredients). The thiol-ene reaction is initiated with the 405 nm UV projection. Then it propagates with bonds formation between thiyl radical and ene functional groups and eventually forms the cross-linked polymer matrix. Due to the amine surface group, the QDs are not likely to be involved in the thiol-ene polymerization, which prevents the phase separation and QDs aggregation. [26] Here we further demonstrate the patterning of light blocking walls between pixels as "black matrix" for color cross-talk reduction, as shown in Fig. 1(b) subplots VI-VIII. The details of exposure time and intensity are listed in the following result sections.

### 2.3. *Instrumentation and characterization*

Fluorescence and white light photos of the printed pattern were taken under a microscope (OMFL600, OMANO) with 100W mercury arc lamp as UV source. The dimensions of patterned pixel array were measured with profilometer (DektakXT, Bruker). Fluorescent emission spectra, peaks and full width at half maximum (FWHM) were measured by spectrofluorometer (Fluorolog-3, Horiba) with integration sphere (Quanta-phi, Horiba) at 400 nm excitation (FWHM of 4 nm). PLQY was calculated following the method developed by de Mello and others. [30] Absorption spectra of the QDs/NOA86 composite was measured with UV-VIS-NIR spectrophotometer (Lambda 1050, Perkin Elmer).

The angular emission intensity was measured with a homemade setup. An optical fiber adapter (SM1SMA, Thorlabs) on a rotation stage was placed 5 cm away from the samples of blue LEDs covered with pixelated color converters, which was centered at the rotation stage. Fluorescent emission collected by the small aperture on the adapter was guided through an optical fiber (QP600-1-VIS-NIR, Ocean Optics) into a spectrometer (USB2000+, Ocean Optics). The angular emission were measured at a step of 5° from −90° to 90° relative to the normal of the sample plane.

Optics EXPRESS

The evaluation of color cross-talk reduction was done by comparing the intensity of flourescence signals (red or green channel values) before and after patterning the light blocking walls between pixelated color converters. The signals were collected by a digital camera (EOS60D, Canon) with fixed shutter speed, aperture and ISO.

## 3. Results and discussion

### 3.1. Patterning results

Figure 2 shows the pixelated QDs/NOA86 color converters patterned by the projection lithography method. The concentration of red and green quantum dots are 100 mg/mL. The exposure time is 1.0 s, and the exposure intensity is 63 mW/cm$^2$. The white light and UV fluorescent microscope pictures show the high patterning resolution with pitch size of 30 μm and pixel size of 21 μm for red pixels as shown in Figs. 2(a)–2(b), and 22 μm for green pixels as shown in Figs. 2(c)–2(d). The size and shape of the pixels could be tuned by adjusting the projected pattern. As shown in Fig. 2(e), square pixels with size from about 40 μm to 6 μm could be achieved. The patterning resolution of the presented mask-less projection lithography system is limited by the pixel size of the DMD chip and the de-magnification factor of the scaling lens system, i.e. the ratio between the equivalent focal lengths of the collimator tube lens and the objective lens. [31] On the other hand, the imaging quality is affected by multiple factors including optical aberration, [31] non-uniformity of the light source illumination on the DMD, [32] exposure dose control over the projected pattern, [33] etc. Applying the same printing procedure with scaling lens system of smaller de-magnification factor and DMD with smaller pixel size can improve the patterning resolution. Meanwhile, aberration-correction, [31] illumination uniformity improvement [32] and gray-scale DMD exposure dose modulation [33] could help to compensate the loss of image quality at lower de-magnification factor. Figure 2(f) shows the capability of patterning pixels with wide range of shape choices, including star, hexagon, circle, triangle and square. All pixels shown in Figs. 2(a)–2(f) were patterned on top glass slides. Figures 2(g)–2(h) demonstrate the capability of multi-material printing for full color conversion with red and green QDs on a blue LED substrate. Figure 2(h) was taken with a 500 nm long pass filter (FEL0500, Thorlabs), under the back illumination of the blue LEDs. Size and color conversion efficiency variance across the patterned pixels could be observed in Figs. 2(g)–2(h). The limitation on uniformity may be caused by the aforementioned factors affecting the image quality. Challenges remain for mass production with full color conversion of such systems despite being demonstrations of blue micro-LED pixels down to 1-2 μm. [34] Further, pixel-level calibration and correction of electrical driving current and optical leakage are required to reduce the overall color conversion variance. [3]

### 3.2. Integration of QDs onto blue LED for color down conversion

We patterned pixelated red and green QDs/NOA86 (QDs concentration of 50 mg/mL) color converters directly on 0.5 mm by 0.5 mm blue LED chips, as shown in Figs. 3(a)–2(b). The fluorescence photos of the red and green pixels excited by the blue LED were taken with 500 nm long pass filter (FEL0500, Thorlabs). The aforementioned patterning procedure resulted in the low-profile shape with thickness below 10 μm for both the red and green pixels. The different thickness of the two types of pixels may come from the mis-focusing of the object lens. Along with the omnidirectional emission properties of QDs, the low-profile pixel shape and the high pixel density benefit the wide angular emission distribution. As shown in Fig. 3(c), the normalized angular emission of both the red and green pixels excited by the blue LED chips approaches the Lambertian emission profile of an ideally diffusive radiator. [35] Fig. 3(d) shows that the fluorescent emission intensity of the red and green pixels can be adjusted by tuning supply voltage to the blue LED chip. The PL intensity was measured with the angular emission

Optics EXPRESS

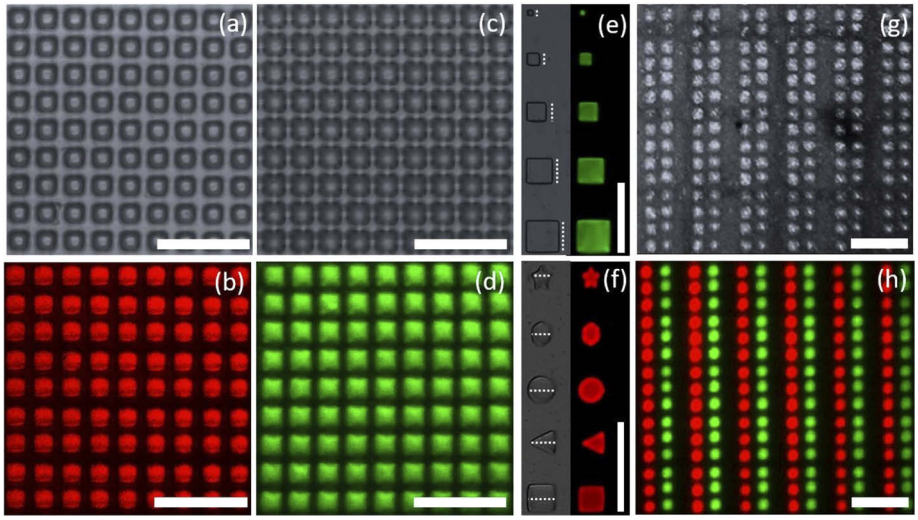


**Fig. 2.** Microscope photos of QDs/NOA86 pixels patterned by projection lithography. (a-d) White light and UV fluorescent images of red as and green square pixels. (e, f) Patterned pixels with various sizes and shapes. The representative feature dimensions are marked by the white dash lines in Figs. 2(e)–2(f). In Fig. 2(e), the dimensions are: 43 μm, 30 μm, 22 μm, 15 μm and 6 μm, from large to small. In Fig. 2(f), the dimensions are: Star: 26 μm; Hexagon: 27μm; Circle: 30 μm; Triangle: 28 μm and Square: 30 μm. (g, h) Direct patterning of multi-color pixels on blue LED substrate. All scale bars are 100 μm.

measurement setup at 0° emission angle, without long pass filtering. Due to the overlap at the range from 475 nm to 500 nm between emission spectrum of the blue LEDs and green QDs/NOA86 pixels, the PL spectrum of the green QDs/NOA86 composite were fitted with Lorentzian function. On the other hand, the emission spectrum of the blue LED was measured without patterning color converters on it. Figure 3(d) indicates that QDs/photo-polymer color converters could be utilized for full color conversion on blue micro-LEDs array by controlling the supply voltage of the nearby micro-LEDs. The wide range of choices for QDs further offers tunability of color gamut for blue LED color down conversion. Figure 3(e) shows the CIE chart of the QDs color converters with the current choice of QDs and photo-polymer matrix, under the assumption of full light conversion from the blue LED. [36] 95% color gamut coverage of the DCI-P3 color space is achievable. [37]

### *3.3. Comparison between QDs/photo-polymer, drop-cast and solution-phase QDs for color down conversion*

The phase separation of QDs/photo-polymer composites at high QDs concentration causes the aggregation of QDs, which increases the non-radiative decay, scattering and re-absorbing of emitted light. [17,28] Those mechanisms result in the reduced PL efficiency, shifted emission peak and expanded emission bandwidth. The rapid thiol-ene photo-polymerization reaction can provide a fast cross-linking process during exposure. [38] It has been shown that QDs/thiol-ene photo-polymer could achieve uniformly dispersed QDs in the polymer matrix at a high QDs loads, without phase separation and QDs aggregation. [26] The NOA optical photo-polymer is also robust for long term operation. [26] In the following of this section, we compare the photo-luminescence of QDs color converters fabricated by conventional solvent drop-casting and projection lithography. The drop-cast QDs were initially dispersed in chloroform of the same

Optics EXPRESS

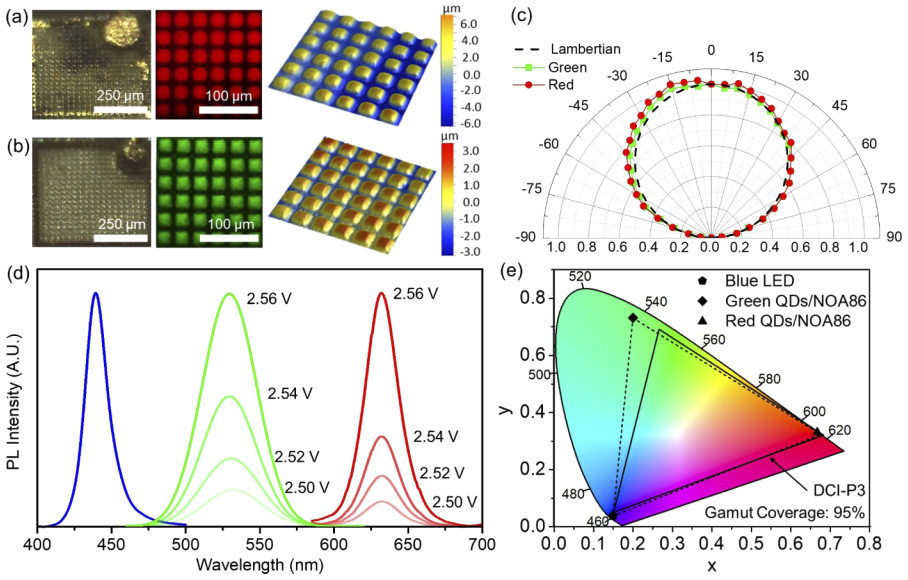


**Fig. 3.** Direct patterning of QDs/NOA86 pixels on blue LEDs for color down conversion. (a, b) White light and PL images and pixelated array profiles of red and green pixels. (c) Angular emission profiles of red and green color converters from blue LED excitation. (d) Blue LED emission spectra (Blue solid line) and PL intensities of green (green solid lines) and red (red solid lines) QDs/NOA86 pixels as increasing the supply voltage on the blue LED chip. (e) Color gamut coverage of the blue LED with red and green QDs color converters. Numbers along the boundary of the chart indicate spectral wavelength of the local colors.

QDs concentrations as the QDs/NOA86 composite. Meanwhile, solution-phase QDs/chloroform suspensions were also measured as references.

Figures 4(a)–4(b) show the absorption of QDs/chloroform suspensions with QDs concentration of 25 mg/mL, as well as the PL emission spectrum of solution-phase QDs, QDs/NOA86 composite and drop-cast QDs at concentration of 25 mg/mL. The PL peaks of drop-cast QDs and QDs/NOA86 composites show red shifts compared to the solution-phase QDs. In Figs. 4(c)–4(d), we further compare the PL emission peaks and FWHM between the three groups of samples at high red or green QDs loads from 25 mg/mL to 100 mg/mL. The PL peaks of solution-phase red and green QDs locate at ~630 nm and ~525 nm separately. The drop-cast QDs show the largest red shifts of the PL peaks (red: ~640 nm and green: ~535 nm), and the widest FWHM (red: ~37 nm and green: ~45 nm), due to the large aggregation after solvent evaporation. [25] On the other hand, the PL peaks of red and green QDs/NOA86 shifted less, at ~632 nm and ~527 nm, with FWHM of ~35 nm and ~40 nm separately, due to the uniform dispersion of QDs in the polymer matrix. The QDs aggregation and host material effects also result in the degradation of PL efficiency. As shown in Figs. 4(e)–4(f), the drop-cast QDs have the lowest PLQY (red: ~11% and green: ~20%) compared to solution-phase (red: ~20% and green: ~40%) and QDs/NOA86 composite (red: ~15% and green: ~35%). We could conclude from this comparison that the photo-lithography patterning of QDs/photo-polymer method outperforms the conventional ink jet or aerosol jet patterning methods by forming a more uniformly dispersed QDs in polymeric matrix. The PLQY of QDs/NOA86 is improved by 0.5-1 times compared to drop-cast QDs. The higher PL efficiency of solution-phase QDs indicates liquid solvents may exceed photo-polymers as host material, which is partly due to the inhibited degradation of QDs passivation. [25,28] Other possible reasons include the light scattering from non-uniform refractive index of the polymer matrix and the high index mismatch between NOA86 (n=1.55) and air. It is suggested

Optics EXPRESS

that strategies like "Stokes-shift-engineered" giant QDs and silica coated QDs could combat the host material effects for QDs/photo-polymer composites. [28,39] On the other hand, liquid phase color conversion pixels is not practical for high-resolution display applications, due to challenges in both manufacturing and maintenance for long lifetime operation. On the other hand, as shown in Figs. 4(e)–4(f), the absorbance coefficient $\mu_a$ of QDs/NOA86 composites (~0.1/μm) are comparable with solution-phase QDs at a high QDs concentration, which is preferable for full blue light conversion within a thin conversion layer. Furthermore, applying optical band pass filters to reflect un-converted blue light back to the luminescence layer can further reduce blue light leakage and increase color gamut for full color conversion. [16]

### 3.4. Color cross-talk reduction with projection lithography patterned black matrix

Color cross-talk may happen due to the blue light leakage between nearby pixels or the unintentional excitation of red QDs by the nearby green QDs. Both of these two mechanisms originate from the coupling of light emitted from pixels into the other nearby pixels. One widely applied technique to reduce color cross-talk due to the unintentional excitation is inserting light blocking walls or "black matrix" between pixels. [20,40] Here we further demonstrate that the projection lithography method could be applied to directly pattern red and green QDs color converters with "black matrix" to reduce color cross-talk.

A black photo-polymer (PR-57 Black, Autodesk) containing light absorbing molecules was used as the black matrix material. First, we followed the previously described procedures to pattern straight lines of red and green color converters (with QDs concentration of 50 mg/mL) on transparent glass substrates. Then the black photo-polymer was applied and exposed with a parallel lines pattern to fill the gap between the nearby pixels. The exposure time is 1.0 s and intensity is 52 mW/cm$^2$.

We compared the color cross-talk of the patterned pixels with and without the black matrix. Figures 5(a)–5(b) show the white light microscope photos in reflection mode of the patterned lines of red and green color converters. The patterned "black matrix" is shown as the white dash rectangular areas in Fig. 5(b). This process can also pattern black matrix walls around square pixels by projecting a grid pattern at the gaps between red and green pixels. It requires a finer alignment between multiple exposure steps, which is limited by the lack of rotational accuracy of the current setup. Figures 5(c)–5(d) show the fluorescence images of the patterned color converters under 405 nm excitation from the UV DMD digital light projector over the whole area. While in Figs. 5(e)–5(f), the excitation only covers the green color converters. The four fluorescence photos were recorded with the same digital camera (EOS60D, Canon) with fixed shutter speed, aperture and ISO. Figures 5(g)–5(h) show the extracted red and green channel intensities from the fluorescence photos, along the white dash lines shown in Figs. 5(c)–5(f). Before and after patterning the black matrix, the green fluorescence emission intensity profiles in both Figs. 5(g)–5(h) keep a similar value, which indicates no direct coverage of the color converters by the black matrix. Furthermore, applying the black matrix in between the red and green color converters effectively reduces the un-intentional excitation of red pixels due to the mitigated coupling of green light emission from a nearby green pixel into the red pixel. As shown in Fig. 5(h), the red channel intensity caused by color cross-talk is reduced by 40% with the black matrix. Further, PL spectrum measurements over larger areas with and without black matrix were conducted by projecting 405 nm excitation light only onto the green color converters. Normalized PL intensity and fitted spectrum with PL centers at 525 nm and 630 nm in Fig. 5(i) confirms that the drop of red PL intensity after adding the black matrix walls, which indicates the color cross-talk reduction. The Projection lithography of black matrix can be a promising solution to prevent color cross-talk between high-resolution QDs converters. However, the continuous decreasing of LED pixels size and pitch distance call the development of new material composites to diminish light coupling between pixels.

Optics EXPRESS

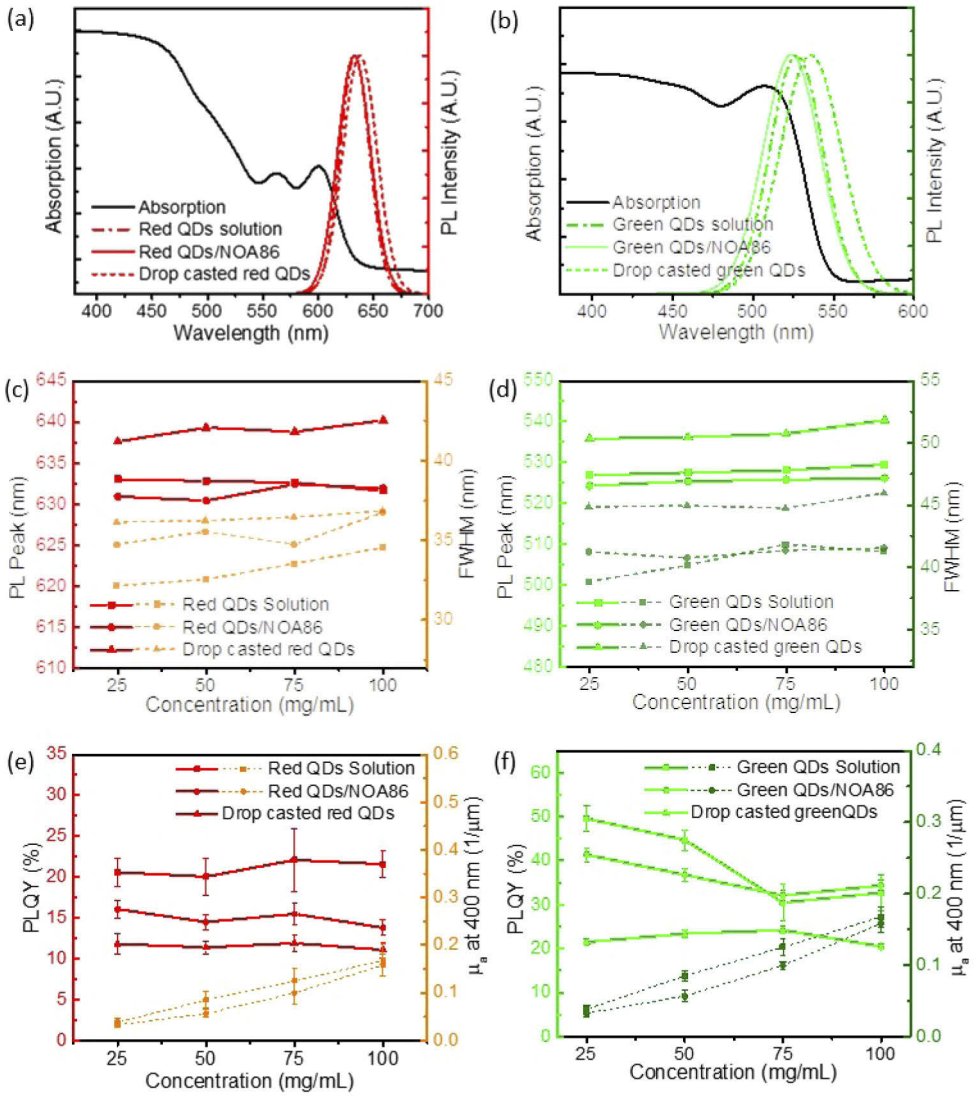


**Fig. 4.** Comparison between QDs/chloroform, QDs/NOA86 composite and drop-cast QDs. (a, b) Absorption and PL emission spectra, with red and green QDs concentration of 25 mg/mL. (c, d) PL peaks and FWHM of the 3 sample groups as increasing the red and green QDs concentration from 25 mg/mL to 100 mg/mL. (e, f) PLQY and absorbance coefficient $\mu_a$ of the 3 sample groups as increasing the red and green QDs concentration from 25 mg/mL to 100 mg/mL.

Optics EXPRESS

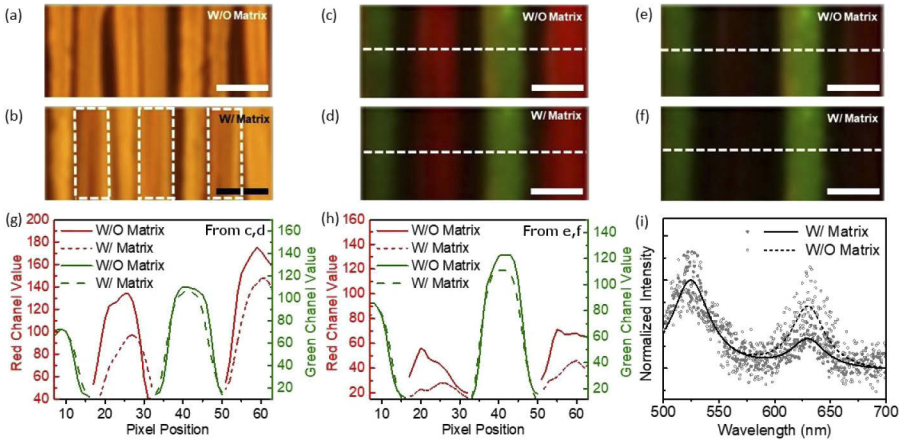


**Fig. 5.** Color cross-talk reduction by projection lithography of "black matrix" in between red and green QDs color converters. (a, b) White light microscope photos of color converters with and without the black matrix. The patterned light absorbing photo-polymer composite is shown as the white dash rectangular areas in Fig. 5(b). (c-f) Fluorescence images of color converters excited by 405 nm light from the UV DLP projector. Figures 5(c) and 5(e) show pixels without black matrix. Figures 5(d) and 5(f) show pixels with black matrix. The UV projection covers the whole area in Figs. 5(c)–5(d), while only covers the green color converters in Figs. 5(e)–5(f). (g) Red and green channel intensities along the white dash lines in Figs. 5(c)–5(d). (h) Red and green color channel intensities along the white dash lines in Figs. 5(e)–5(f). All scale bars are 25 μm. (i) Normalized PL intensity and fitted PL spectrum of areas with and without black matrix.

## 4. Conclusion

In summary, we demonstrated the direct patterning of QDs/thiol-ene photo-polymer composite as high-resolution pixelated color converters with DLP projection lithography method. Square pixels array of 21 μm size, 30 μm pitch and sub 10 μm thickness was demonstrated. The smallest pixel size of 6 μm printed by this method has not been achieved by ink-jet or aerosol jet methods. The fast thiol-ene photo-polymerization reaction facilitates the uniform dispersion of highly concentrated amine capped QDs in the polymer matrix, which improves PLQY by 0.5-1 times compared to solvent drop-cast QDs. Meanwhile the advantages of QDs as color converters for wide viewing angle and wide gamut are maintained. A nearly ideal diffusive angular emission with 95% gamut coverage of DCI-P3 standard are achievable. The DLP projection lithography method also offers promising solutions to resolve the color cross-talk due to the leakage of omnidirectional emission from QDs. The combination of QDs/photo-polymer with projection lithography patterning method presents great potential for high-resolution and efficient color conversion in applications like high-end lighting and display, visible light communication and optogenetic neural controls.

## Funding

OSRAM-MIT Joint Research; Directorate for Engineering (DMR1419807); Army Research Office (W911NF-13-D-0001).

## Acknowledgments

X.L., Z.J.T. and N.F. acknowledge the Center for Materials Science and Engineering (CMSE) and the Institute for Soldiers Nanotechnology (ISN) shared facilities as part of Massachusetts Institute

Optics EXPRESS

of Technology. UV-VIS-NIR spectrometry and profilometry measurements were performed at CMSE, which is supported by the National Science Foundation under Grant No. DMR1419807. Spectrofluorometry measurements were performed at ISN, which was supported by the US Army Research Office under contract number W911NF-13-D-0001.

## References

1. B. Xie, R. Hu, and X. Luo, "Quantum dots-converted light-emitting diodes packaging for lighting and display: status and perspectives," J. Electron. Packag. **138**(2), 020803 (2016).
2. T. Wu, C.-W. Sher, Y. Lin, C.-F. Lee, S. Liang, Y. Lu, S.-W. Huang Chen, W. Guo, H.-C. Kuo, and Z. Chen, "Mini-LED and micro-LED: promising candidates for the next generation display technology," Appl. Sci. **8**(9), 1557–1573 (2018).
3. K. Ding, V. Avrutin, N. Izyumskaya, Ü. Özgür, and H. Morkoç, "Micro-LEDs, a manufacturability perspective," Appl. Sci. **9**(6), 1206–1220 (2019).
4. S. Groetsch, J. Reill, M. Schwind, S. Haneder, and U. Hiller, "Illumination vs. visualization in headlamps: Way towards hd light source requirements," in *Proc. SIA VISION 2018*, (SIA, 2018).
5. D. Kundaliya, N. von Malm, and K. Mishra, "Integration of YAG: Ce thin film wavelength converter on III-V blue LED via a laser lift-off process," ECS J. Solid State Sci. Technol. **7**(1), R3046–R3051 (2018).
6. M. S. Islim, R. X. Ferreira, X. He, E. Xie, S. Videv, S. Viola, S. Watson, N. Bamiedakis, R. V. Penty, I. H. White, A. E. Kelly, E. Gu, H. Haas, and M. D. Dawson, "Towards 10 gb/s orthogonal frequency division multiplexing-based visible light communication using a GaN violet micro-LED," Photonics Res. **5**(2), A35–A43 (2017).
7. S. Mei, X. Liu, W. Zhang, R. Liu, L. Zheng, R. Guo, and P. Tian, "High-bandwidth white-light system combining a micro-LED with perovskite quantum dots for visible light communication," ACS Appl. Mater. Interfaces **10**(6), 5641–5648 (2018).
8. D. Xue, C. Ruan, Y. Zhang, H. Chen, X. Chen, C. Wu, C. Zheng, H. Chen, and W. Y. William, "Enhanced bandwidth of white light communication using nanomaterial phosphors," Nanotechnology **29**(45), 455708 (2018).
9. N. McAlinden, D. Massoubre, E. Richardson, E. Gu, S. Sakata, M. D. Dawson, and K. Mathieson, "Thermal and optical characterization of micro-LED probes for in vivo optogenetic neural stimulation," Opt. Lett. **38**(6), 992–994 (2013).
10. S. Ayub, C. Gossler, F. Engesser, O. Paul, and P. Ruther, "Compact intracerebral probe with yellow phosphor-based light conversion for optogenetic control," in *2017 19th International Conference on Solid-State Sensors, Actuators and Microsystems (TRANSDUCERS)*, (IEEE, 2017), pp. 1703–1706.
11. B. Ji, Z. Guo, M. Wang, B. Yang, X. Wang, W. Li, and J. Liu, "Flexible polyimide-based hybrid opto-electric neural interface with 16 channels of micro-LEDs and electrodes," Microsyst. Nanoeng. **4**(1), 27 (2018).
12. S. Coe-Sullivan, W. Liu, P. Allen, and J. S. Steckel, "Quantum dots for LED downconversion in display applications," ECS J. Solid State Sci. Technol. **2**(2), R3026–R3030 (2013).
13. J. S. Steckel, J. Ho, C. Hamilton, J. Xi, C. Breen, W. Liu, P. Allen, and S. Coe-Sullivan, "Quantum dots: The ultimate down-conversion material for LCD displays," J. Soc. Inf. Disp. **23**(7), 294–305 (2015).
14. M. J. Smith, C. H. Lin, S. Yu, and V. V. Tsukruk, "Composite structures with emissive quantum dots for light enhancement," Adv. Opt. Mater. **7**(4), 1801072 (2019).
15. F. Gou, E.-L. Hsiang, G. Tan, Y.-F. Lan, C.-Y. Tsai, and S.-T. Wu, "High performance color-converted micro-LED displays," J. Soc. Inf. Disp. **27**(4), 199–206 (2019).
16. H.-V. Han, H.-Y. Lin, C.-C. Lin, W.-C. Chong, J.-R. Li, K.-J. Chen, P. Yu, T.-M. Chen, H.-M. Chen, K.-M. Lau, and H.-C. Kuo, "Resonant-enhanced full-color emission of quantum-dot-based micro LED display technology," Opt. Express **23**(25), 32504–32515 (2015).
17. H.-J. Kim, M.-H. Shin, H.-G. Hong, B.-S. Song, S.-K. Kim, W.-H. Koo, J.-G. Yoon, S.-Y. Yoon, and Y.-J. Kim, "Enhancement of optical efficiency in white OLED display using the patterned photoresist film dispersed with quantum dot nanocrystals," J. Disp. Technol. **12**(6), 526–531 (2016).
18. B. H. Kim, M. S. Onses, J. B. Lim, S. Nam, N. Oh, H. Kim, K. J. Yu, J. W. Lee, J.-H. Kim, S.-K. Kang, C. H. Lee, J. Lee, J. H. Shin, N. H. Kim, C. Leal, M. Shim, and J. Roger, "High-resolution patterns of quantum dots formed by electrohydrodynamic jet printing for light-emitting diodes," Nano Lett. **15**(2), 969–973 (2015).
19. B. Bao, M. Li, Y. Li, J. Jiang, Z. Gu, X. Zhang, L. Jiang, and Y. Song, "Patterning fluorescent quantum dot nanocomposites by reactive inkjet printing," Small **11**(14), 1649–1654 (2015).
20. H.-Y. Lin, C.-W. Sher, D.-H. Hsieh, X.-Y. Chen, H.-M. P. Chen, T.-M. Chen, K.-M. Lau, C.-H. Chen, C.-C. Lin, and H.-C. Kuo, "Optical cross-talk reduction in a quantum-dot-based full-color micro-light-emitting-diode display by a lithographic-fabricated photoresist mold," Photonics Res. **5**(5), 411–416 (2017).
21. E. Lee, S. Kan, C. Hotz, J. Yurek, Z. Luo, H. Kim, J. Yamanaga, and A. Carpenter, "67-2: Invited paper: Ambient processing of quantum dot photoresist for emissive displays," in *SID Symposium Digest of Technical Papers*, (Wiley Online Library, 2017), pp. 984–987.
22. S. Lee and C. Lee, "High-density quantum dots composites and its photolithographic patterning applications," Polym. Adv. Technol. **30**(3), 749–754 (2019).

Optics EXPRESS


23. M. Kneissl, T. Kolbe, C. Chua, V. Kueller, N. Lobo, J. Stellmach, A. Knauer, H. Rodriguez, S. Einfeldt, Z. Yang, N. M. Johson, and M. Weyers, "Advances in group III-nitride-based deep UV light-emitting diode technology," Semicond. Sci. Technol. **26**(1), 014036 (2010).
24. L. Dupré, M. Marra, V. Verney, B. Aventurier, F. Henry, F. Olivier, S. Tirano, A. Daami, and F. Templier, "Processing and characterization of high resolution GaN/InGaN LED arrays at 10 micron pitch for micro display applications," in *Gallium Nitride Materials and Devices XII*, (International Society for Optics and Photonics, 2017), pp. 1010422–1010429.
25. S. Sadeghi, B. G. Kumar, R. Melikov, M. M. Aria, H. B. Jalali, and S. Nizamoglu, "Quantum dot white LEDs with high luminous efficiency," Optica **5**(7), 793–802 (2018).
26. M. J. Smith, S. T. Malak, J. Jung, Y. J. Yoon, C. H. Lin, S. Kim, K. M. Lee, R. Ma, T. J. White, T. J. Bunning, Z. L. Lin, and V. V. Tsukruk, "Robust, uniform, and highly emissive quantum dot–polymer films and patterns using thiol–ene chemistry," ACS Appl. Mater. Interfaces **9**(20), 17435–17448 (2017).
27. T. Zhou, B. Zhang, Y. Qi, D. Xie, J. Yao, Z. Cao, and J. Xue, "P-92: Fabrication and patterning of a wide-color-gamut color filter based on quantum dots," in *SID Symposium Digest of Technical Papers*, (Wiley Online Library, 2016), pp. 1469–1471.
28. H. Li, K. Wu, J. Lim, H.-J. Song, and V. I. Klimov, "Doctor-blade deposition of quantum dots onto standard window glass for low-loss large-area luminescent solar concentrators," Nat. Energy **1**(12), 16157 (2016).
29. F. Gou, E.-L. Hsiang, G. Tan, Y.-F. Lan, C.-Y. Tsai, and S.-T. Wu, "Tripling the optical efficiency of color-converted micro-LED displays with funnel-tube array," Crystals **9**(1), 39–48 (2019).
30. J. C. de Mello, H. F. Wittmann, and R. H. Friend, "An improved experimental determination of external photoluminescence quantum efficiency," Adv. Mater. **9**(3), 230–232 (1997).
31. Y.-H. Liu, Y.-Y. Zhao, X.-Z. Dong, M.-L. Zheng, F. Jin, J. Liu, X.-M. Duan, and Z.-S. Zhao, "Multi-scale structure patterning by digital-mask projective lithography with an alterable projective scaling system," AIP Adv. **8**(6), 065317 (2018).
32. Z. Xiong, H. Liu, R. Chen, J. Xu, Q. Li, J. Li, and W. Zhang, "Illumination uniformity improvement in digital micromirror device based scanning photolithography system," Opt. Express **26**(14), 18597–18607 (2018).
33. Q. Deng, Y. Yang, H. Gao, Y. Zhou, Y. He, and S. Hu, "Fabrication of micro-optics elements with arbitrary surface profiles based on one-step maskless grayscale lithography," Micromachines **8**(10), 314–325 (2017).
34. E. H. Virey and N. Baron, "Status and prospects of microLED displays," in *SID Symposium Digest of Technical Papers*, vol. 49 (Wiley Online Library, 2018), pp. 593–596.
35. F. L. Pedrotti, L. M. Pedrotti, and L. S. Pedrotti, *Introduction to Optics* (Cambridge University, 2017).
36. T. Smith and J. Guild, "The CIE colorimetric standards and their use," Trans. Opt. Soc., London **33**(3), 73–134 (1931).
37. *D-Cinema Quality-Reference Projector and Environment* (SMPTE Recommended Practice, 2011).
38. A. B. Lowe, "Thiol-ene click reactions and recent applications in polymer and materials synthesis," Polym. Chem. **1**(1), 17–36 (2010).
39. F. Meinardi, A. Colombo, K. A. Velizhanin, R. Simonutti, M. Lorenzon, L. Beverina, R. Viswanatha, V. I. Klimov, and S. Brovelli, "Large-area luminescent solar concentrators based on stokes-shift-engineered nanocrystals in a mass-polymerized pmma matrix," Nat. Photonics **8**(5), 392–399 (2014).
40. R. W. Sabnis, "Color filter technology for liquid crystal displays," Displays **20**(3), 119–129 (1999).